Conference Proceedings of the Society for Experimental Mechanics Series

Fikret Necati Catbas *Editor*

Dynamics of Civil Structures, Volume 4

Proceedings of the 32nd IMAC, A Conference and Exposition on Structural Dynamics, 2014

SEM

Springer

Fikret Necati Catbas
Editor

Dynamics of Civil Structures, Volume 4

Proceedings of the 32nd IMAC, A Conference and Exposition on Structural Dynamics, 2014

Springer

Editor
Fikret Necati Catbas
Engineering Department
University of Central Florida
Orlando, FL, USA

ISSN 2191-5644 ISSN 2191-5652 (electronic)
ISBN 978-3-319-04545-0 ISBN 978-3-319-04546-7 (eBook)
DOI 10.1007/978-3-319-04546-7
Springer Cham Heidelberg New York Dordrecht London

Library of Congress Control Number: 2014935871

Printed on acid-free paper

Springer is part of Springer Science+Business Media (www.springer.com)

Preface

Dynamics of Civil Structures, Volume 4 represents one of the eight volumes of technical papers presented at the 32nd IMAC, A Conference and Exposition on Structural Dynamics, 2014, organized by the Society for Experimental Mechanics, and held in Orlando, Florida, February 3–6, 2014. The full proceedings also include volumes on Dynamics of Coupled Structures; Nonlinear Dynamics; Model Validation and Uncertainty Quantification; Structural Health Monitoring; Special Topics in Structural Dynamics; Topics in Modal Analysis I; and Topics in Modal Analysis II.

Each collection presents early findings from experimental and computational investigations on an important area within structural dynamics. Dynamics of civil structures is one of these areas.

The Dynamics of Civil Structures Technical Division serves as a primary focal point within the SEM umbrella for technical activities devoted to civil structures testing, monitoring, and assessment. This volume covers dynamic testing and analysis of all kinds of civil engineering structures such as buildings, bridges, stadiums, and dams. Over the last few years, there has been an interest in input and output modal analysis, as well as output only, ambient vibration testing of bridges. In addition to the material in this volume, a number of technical contributions devoted to new methods, nonlinear dynamics, wind turbine dynamics, and monitoring related to civil structure dynamics may be found in other volumes of these proceedings.

The organizers would like to thank the authors, presenters, session organizers, and session chairs for their participation in this track.

Orlando, FL, USA

Fikret Necati Catbas

Contents

1 **Automatic Modal Identification Based on Narrow-Band Algorithms** 1
Tong Wang, F. Necati Catbas, and Lingmi Zhang

2 **Cable Parameters for Homogenous Cable-Beam Models for Space Structures** 7
Kaitlin Spak, Gregory Agnes, and Daniel Inman

3 **Numerical Continuation Methods for the Concept of Non-linear Normal Modes** 19
Martin Jerschl, Dominik Süß, and Kai Willner

4 **Strategies for Coupled Vibration Suppression and Energy Harvesting** 27
A. Cammarano, A. Gonzalez-Buelga, S.A. Neild, D.J. Inman, and S.G. Burrow

5 **Expansion of Mode Shapes and Responses on the Offshore Platform Valdemar** 35
Anders Skafte, Ulf Tyge Tygesen, and Rune Brincker

6 **Vibration Testing of a Floor During Multiple Phases of Construction** 43
Brad Pridham

7 **Investigation of a Slab on Grade Supporting Sensitive Equipment** 53
B.R. Barben and L.M. Hanagan

8 **Experimental Modal Analysis of a Prestressed Concrete Double-Tee Joist Roof Subject to Blast** 61
Timothy P. Kernicky, Matthew J. Whelan, and David C. Weggel

9 **Structural Evaluation of an Earthen Building from Operational Modal Analysis** 71
Rafael Aguilar, Mario Solís, César Chácara, and Álvaro Ruiz

10 **Smart Sensor Nodes for Vibration Measurement of Large Civil Infrastructure** 81
Jong-Jae Lee, Young-Soo Park, Won-Tae Lee, and Chang-Geun Lee

11 **Floor Vibrations on Healthcare Facilities: A Case Study on a Surgical Microscope** 91
Omer F. Tigli

12 **Modeling Human –Structure Interaction Using a Close Loop Control System** 101
Albert R. Ortiz Lasprilla, Juan M. Caicedo, and Gustavo A. Ospina

13 **Damage Localisation Using Symbolic Time Series Approach** 109
Mehrisadat Makki Alamdari, Jianchun Li, and Bijan Samali

14 **Automated Structural Damage Detection Using One-Class Machine Learning** 117
James Long and Oral Buyukozturk

15 **Interaction Between Humans and Structures** 129
Lars Pedersen

16 **Effects of Human –Structure Interaction from Seated Occupants on a Cantilevered Laboratory Test Structure** 135
Kelly A. Salyards and William Brennan III

17 **Investigating Predicted Floor Response Sensitivity to Input Forcing Function Variables** 145
Julia M. Graham and J. Shayne Love

18 **Vibration Performance of Bridges Made of Fibre Reinforced Polymer** 155
S. Živanović, G. Feltrin, J.T. Mottram, and J.M.W. Brownjohn

19 **Characterization of Human Motion Through Floor Vibration** 163
J.M. Hamilton, B.S. Joyce, M.E. Kasarda, and P.A. Tarazaga

20 **Vision-Based Tracking of Human Body Motion** 171
Feng Zheng, Vitomir Racic, James M.W. Brownjohn, Mark T. Elliot, and Alan Wing

21 **Mathematical Framework for Real-Time Hybrid Substructuring of Marine Structural Systems** 175
Rui M. Botelho and Richard E. Christenson

22 **Damage Detection in Civil Engineering Structure Considering Temperature Effect** 187
V.H. Nguyen, J. Mahowald, J.-C. Golinval, and S. Maas

23 **Damage Detection on the Z24 Bridge by a Spectral-Based Dynamic Identification Technique** 197
Maria G. Masciotta, Luís F. Ramos, Paulo B. Lourenço, and Marcello Vasta

24 **Nonlinear Harmonic Identification of Cracks in Structures** 207
Oliviero Giannini, Paolo Casini, and Fabrizio Vestroni

25 **A Strategy for Improving Performance in Real Time Hybrid Testing** 219
Jonathan L. du Bois

26 **Development and Performance Analysis of Single Axis Simulation Table for Durability Testing** 227
S. Doranga and C.Q. Wu

27 **Comparative Study of Uncertainty Quantification Metrics via a Stochastic Method of Model Validation** ... 235
Sifeng Bi, Sez Atamturktur, and Zhongmin Deng

28 **Nonlinear Identification of a Seven-Story Shear Wall Building Based on Numerically Simulated Seismic Data** 245
Eliyar Asgarieh, Babak Moaveni, Amin Nozari, Andre R. Barbosa, and Eleni Chatzi

29 **Structural Identification Using the Applied Element Method: Advantages and Case Study Application** 255
Matthew J. Whelan, Timothy P. Kernicky, and David C. Weggel

30 **Modal Scaling in OMA Using the Mass matrix of a Finite Element Model** 263
M.L. Aenlle and R. Brincker

31 **Identifying Structural Parameters of an Idling Offshore Wind Turbine Using Operational Modal Analysis** 271
Paul L.C. van der Valk and Marco G.L. Ogno

32 **Dynamic Behavior of Laminated Glass Beams** 283
Manuel L. Aenlle, Alberto Nieto Marrón, and Pelayo Fernández

33 **Modal Identification of Golden Gate Bridge Using Pseudo Mobile Sensing Data with STRIDE** 293
Thomas J. Matarazzo and Shamim N. Pakzad

34 **Removing the Influence of Rotor Harmonics for Improved Monitoring of Offshore Wind Turbines** 299
S. Manzato, C. Devriendt, W. Weijtjens, E. Di Lorenzo, B. Peeters, and P. Guillaume

35 **Evaluating Different Automated Operational Modal Analysis Techniques for the Continuous Monitoring of Offshore Wind Turbines** 313
Mahmoud El-Kafafy, Christof Devriendt, Wout Weijtjens, Gert De Sitter, and Patrick Guillaume

36 **Cable Tension Estimation Using Vision-Based Monitoring System Under Weather Conditions** 331
Sung-Wan Kim, Nam-Sik Kim, Young-Min Kim, and Jong-Chil Park

37 **Direct Structural Damping Identification Method** 341
V. Arora

38 **Modal Analysis and Numerical Models of a Typical Railway Bridge** 351
Volkmar Zabel and Jens Gössinger

39 **Modal and Structural Identification of a Skew, Cable Stayed, Arch Bridge** 359
R. Alaggio, F. Benedettini, M. Dilena, and A. Morassi

40 **A Dynamic Model for Truck-Induced Vibrations on a Cable-Stayed Bridge** 369
T. Argentini, E. Sabbioni, and M. Vignati

41 **Numerical Modeling and Dynamic Testing on the Oglio Flyover of the New BreBeMi Highway in Italy** 381
Alfredo Cigada, Elena Mola, Simona Moschini, Murathan Ahmet Paksoy, Chiara Pozzuoli, and Marcello Vanali

42 **Comparative Evaluation of Excitation Schemes for Multi-Shaker Testing of Bridges** 395
Eric V. Fernstrom and Kirk A. Grimmelsman

43 **Ambient Vibration Testing of the Eureka-Samoa Channel Bridge** 403
Martin Turek, Carlos E. Ventura, Jason Dowling, Sheri Molnar, and Yavuz Kaya

44 **Ambient Vibration Testing of the Painter St. Overpass** 411
Martin Turek, Carlos E. Ventura, Jason Dowling, Sheri Molnar, and Yavuz Kaya

45 **Natural Frequencies of Long-Span Suspension Bridges Subjected to Aerodynamic Loads** 419
G. Piana, A. Manuello, R. Malvano, and A. Carpinteri

46 **Seismic Response Control of Adjacent Buildings Connected by Viscous and Hybrid Dampers** 433
Luis Alejandro Pérez, Suzana Avila, and Graciela Doz

47 **Comparing Statistical Classification with a Vibro-Tactile Human–Machine Interface for Structural Health Monitoring** 441
Jessica Block, Stephanie Djidjev, N. Jordan Jameson, and David Mascarenas

48 **Modal Identification Tests on Archaeological Heritage: The Case of Chokepukio** 451
Rafael Aguilar, Karim Sovero, Carol Martel, and César Chácara

49 **Fluid-Structure Interaction Analysis of Vibration Reduction in Pipe Systems** 459
Peter Persson, Kent Persson, and Göran Sandberg

50 **Application of Positive Position Feedback Control Schemes in a Building-Like Structure** 469
G. Silva-Navarro, J. Enríquez-Zárate, and M.E. Belandria-Carvajal

51 **Active Control of Three-Dimensional Structures** 479
Arcan Yanik, Unal Aldemir, and Mehmet Bakioglu

52 **Dynamic Vibration Absorber Design for a Motor and Pump Assembly** 487
C.B. Nel and J. van Wyngaardt

53 **Design and Performance Analysis of Inerter-Based Vibration Control Systems** 493
Irina F. Lazar, Simon A. Neild, and David J. Wagg

54 **Using Tuned Mass Dampers to Control Imperceptible Motions** 501
Michael J. Wesolowsky, Allan L. Raun, Ramin Behboudi, and John C. Swallow

55 **A Simplified Approach for the Dynamic Analysis of High-Rise Structures** 509
Alberto Carpinteri and Sandro Cammarano

56 **A Machine Learning Approach to Nonlinear Modal Analysis** 521
K. Worden and P.L. Green

Chapter 1
Automatic Modal Identification Based on Narrow-Band Algorithms

Tong Wang, F. Necati Catbas, and Lingmi Zhang

Abstract A procedure for the automatic modal identification based on Narrow-Band algorithms is presented in this paper. The Lagrange interpolation polynomial is firstly utilized to find the modal peaks automatically. Then the modal assurance criterion values between adjacent modal vectors are calculated to decide the fitting band automatically. The procedure can be applied to Narrow-Band algorithms both for experimental and operational modal analysis. The result of automatic identification of real life testing and experimental data is finally demonstrated.

Keywords Automatic identification • Narrow-band • Automatic peak finding • Experimental modal analysis • Operational modal analysis

1.1 Introduction

The technique of modal analysis has been developing for more than three decades. There are two types of modal analysis: one is Experimental Modal Analysis (EMA), and the other is Operational Modal Analysis (OMA). Both input (excitation) and output (response) signals are utilized in EMA, while only the output responses are used in OMA. Since EMA is generally conducted in a lab with good experimental environment, the data acquired is usually of high signal to noise ratio (SNR), and good identification result could be obtained. In some field conditions, the tested structures cannot be artificially excited, therefore only the responses from the natural loadings such as wind and traffic can be utilized to extract the modal parameters.

The identification algorithms for modal analysis can be classified into three types: Narrow-Band, Select-Band and Broad-Band. The Narrow-Band algorithms identify modes one by one, among which the most typical algorithm is CMIF (Complex Mode Indicator Function) [1] for EMA and FSDD (Frequency Spatial Domain Decomposition) [2] for OMA. The Select-Band algorithms identify several modes from one or several selected frequency bands in one time. The well-known FDPR (Frequency Domain Poly-References) [3] and RFOP (Rational Fraction Orthogonal Polynomials) [4] algorithms both belong to that type. The Broad-Band algorithm can identify modes in a broad frequency band or even the full band. The most famous broad band algorithm is pLSCF (poly-reference Least Squares Complex Frequency domain) [5] or so-called polyMAX.

The Narrow-Band algorithms are now widely applied, because they are proved to be easy-to-use and very powerful. Especially in the operational analysis for large-scale civil engineering structures such as buildings and bridges, the FSDD shows great advantages [6]. However, compared to other kinds of modal identification algorithms, more interactions and time are needed to complete the whole analysis: the peaks have to be selected one by one, and the fitting bands for each modes have to be set and adjusted manually to get better result. An auto identification method will be great to the structural health monitoring (SHM) [7].

T. Wang (✉) • L. Zhang
State Key Laboratory of Mechanics and Control of Mechanical Structures, Nanjing University of Aeronautics and Astronautics, 29 Yudao Street, Nanjing 210016, China
e-mail: wt78@nuaa.edu.cn

F.N. Catbas
Department of Civil, Environmental and Construction Engineering, University of Central Florida, 4000 Central Florida Blvd, Orlando, FL 32816, USA
e-mail: catbas@ucf.edu

F.N. Catbas (ed.), *Dynamics of Civil Structures, Volume 4: Proceedings of the 32nd IMAC, A Conference and Exposition on Structural Dynamics, 2014*, Conference Proceedings of the Society for Experimental Mechanics Series,
DOI 10.1007/978-3-319-04546-7_1,

In this paper, a procedure for the automatic modal identification based on Narrow-Band algorithms is presented. The Lagrange interpolation polynomial is firstly utilized to pick the modal peaks automatically. Then the modal assurance criterion values between adjacent modal vectors are calculated to decide the fitting band automatically. The procedure can be applied to Narrow Band algorithms both for experimental and operational modal analysis. Two application examples are demonstrated to validate the procedure: an EMA test of an aircraft model and an OMA test of a 15-story office building.

1.2 The Mode Indicator Function

The Narrow-Band algorithms are based on the Mode Indication Function (MIF), which is defined as the singular values of the frequency response function (FRF) matrix in EMA or power spectrum density (PSD) matrix in OMA.

$$FRF\,(j\omega) = U\Sigma V^H \tag{1.1}$$

$$PSD\,(j\omega) = U\Sigma U^H \tag{1.2}$$

In the above equations U and V are the singular vector matrices, and Σ is the singular value matrix. The mode indicator functions consists of the singular values in Σ matrix at each spectral line. Note that in OMA, the PSD matrix are always a square matrix.

The peaks in the MIF plot indicate the existence of modes, and the peak frequencies give the approximate estimation of the damped natural frequencies. The magnitude of specific modal peak is relative to the strength of the mode. The mode shape vectors can also be obtained from the corresponding singular vectors. Therefore, the modes can be automatically detected by applying some automatic peak-finding algorithms on the MIF plots.

1.3 Automatic Peaks Finding

There are many methods for the auto peak finding, such as Local Maximum method, First Derivative method and Second Derivative method. The simplest way is to find the maximum value in a selected band. It is suitable for the case that only one mode is available. A more common way is to make use of the fact that the first derivative of a peak has a downward-going zero-crossing at the peak maximum. Another method is based on the law that the second derivative of a peak has a local minimum value. However, due to the presence of noise in the real signal, besides the real signal peaks, many other false peaks may be found. To avoid this problem, the signal could be smoothed, and a magnitude threshold of peak values could be set.

In this paper, the first derivative method is used to find peaks automatically. For the sake of getting better estimation of numerical differentiation, the four-order Lagrange interpolation polynomial is applied to calculate the derivative. Five adjacent points should be included for the construction of a four-order Lagrange polynomial. Assuming five points located at $(x_0, f(x_0))$, $(x_1, f(x_1))$, $(x_2, f(x_2))$, $(x_3, f(x_3)$ and $(x_4, f(x_4))$, we can write the four-order Lagrange polynomial as:

$$P_4\,(x_0 + th) = \sum_{i=0}^{4} \left(\left(\prod_{\substack{j=0 \\ j \neq i}}^{4} \frac{t-j}{i-j} \right) f\,(x_i) \right) \tag{1.3}$$

where h is the x interval: $h = x_{k+1} - x_k$, and t is 0, 1, 2, 3 and 4 respectively. Then the derivation of the polynomial can be obtained:

$$\begin{aligned} P_4'\,(x_0 + th) = {} & \frac{(4t^3-30t^2+70t-50)}{24h} f\,(x_0) - \frac{(4t^3-27t^2+50t-24)}{6h} f\,(x_1) \\ & + \frac{(4t^3-26t^2+38t-12)}{4h} f\,(x_2) - \frac{(4t^3-21t^2+26t-8)}{6h} f\,(x_3) \\ & + \frac{(4t^3-18t^2+20t-6)}{24h} f\,(x_4) \end{aligned} \tag{1.4}$$

By taking Eq. (1.4), the first derivate values at the five points can be estimated. The peaks can be detected by checking the downward-going zero-crossing parts in the first derivate data array. In order to reduce the number of false peaks, a proper peak magnitude threshold value can be set.

1.4 Automatic Curve Fitting

To get the accurate modal frequency and damping ratio in a Narrow-Band identification algorithm, the modal enhancement is required. It could be proved that the in the vicinity of the modal peak, the enhanced FRF/PSD can be decoupled to a single degree of freedom FRF/PSD.

In the CMIF algorithm, an enhanced FRF for the r^{th} mode can be defined as:

$$\widehat{H}(j\omega) = u_r^H FRF(j\omega) v_r \tag{1.5}$$

And in the FSDD algorithm, an enhanced PSD for the r^{th} mode can be defined as:

$$\widehat{G}(j\omega) = u_r^H PSD(j\omega)^T u_r \tag{1.6}$$

Where U_r and V_r are the corresponding singular vectors to the specified modal peak in the mode indicator function.

The modal frequency and damping ratio can be obtained by the least-square fitting to the enhanced FRF or PSD. The coherence between the singular vector at the peak and the singular vector at the neighboring spectral lines can be estimated by calculating the Modal Assurance Criterion (MAC).

$$MAC = \frac{\left|U_r^H U_j\right|^2}{U_r^H U_r U_j^H U_j} \tag{1.7}$$

Here U_j is a singular vector at one adjacent spectral line. If there is only one dominant mode in the enhanced FRF/PSD, the MAC value should be close to unity. The farther the spectral line from the peak, the smaller the MAC value is. Therefore, by setting a MAC threshold such as 0.8, it is possible to determine a reasonable fitting band.

1.5 Auto Identification of an Aircraft Model

A delta-shaped aircraft model is utilized as an EMA application example for automatic Narrow-Band modal identification. The model is made of aluminum with dimension of 1,240 mm in length and 1,100 mm in wing span. A hammer impact test with two reference accelerometers and 41 roving impact DOFs was performed to do the modal analysis. A FRF matrix with 800 spectrum lines was obtained by the signal processing. The modal indicator function estimated from the FRF matrix is showed in Fig. 1.1.

By applying the auto peak finding procedure described as above, eight modes are detected, including the first one as a rigid body mode. As shown in Fig. 1.2, the downward-going zero-crossing positions in the first derivative indicate the modal peaks in the modal indicator function very clearly.

Figure 1.3 shows the enhanced FRF of the one mode at 57 Hz. The curve fitting band between two vertical lines is automatically determined by setting a MAC threshold of 0.8. The identified modal frequencies and damping ratios are shown in Table 1.1.

1.6 Auto Identification of CFT Building

The auto identification procedure was also applied to a 15-story office building with concrete-filled-tube (CFT) located in Tokyo. The field ambient accelerations of 53 measurement degree of freedoms were acquired with 14 accelerometers in four groups, with two as references. The FSDD Narrow-Band algorithm is utilized to do the operational modal analysis. The PSD matrix was first calculated, and then the mode indicator functions were estimated by the singular value decomposition.

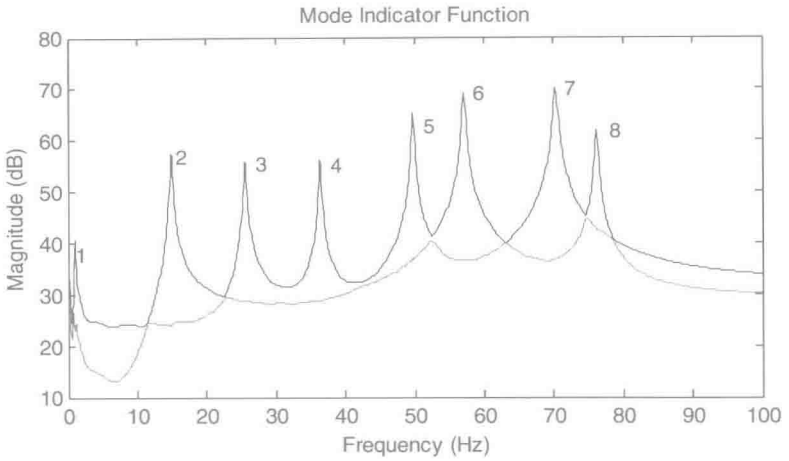

Fig. 1.1 Peaks found in the mode indicator function of the aircraft model

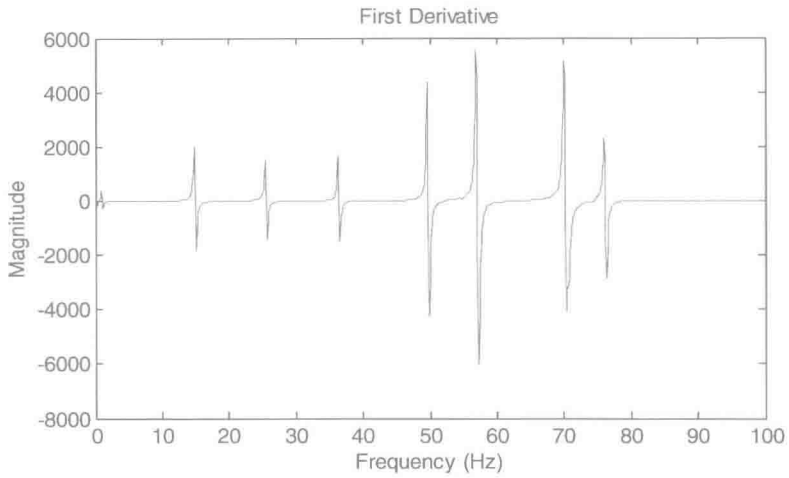

Fig. 1.2 First derivative of the mode indicator function of the aircraft model

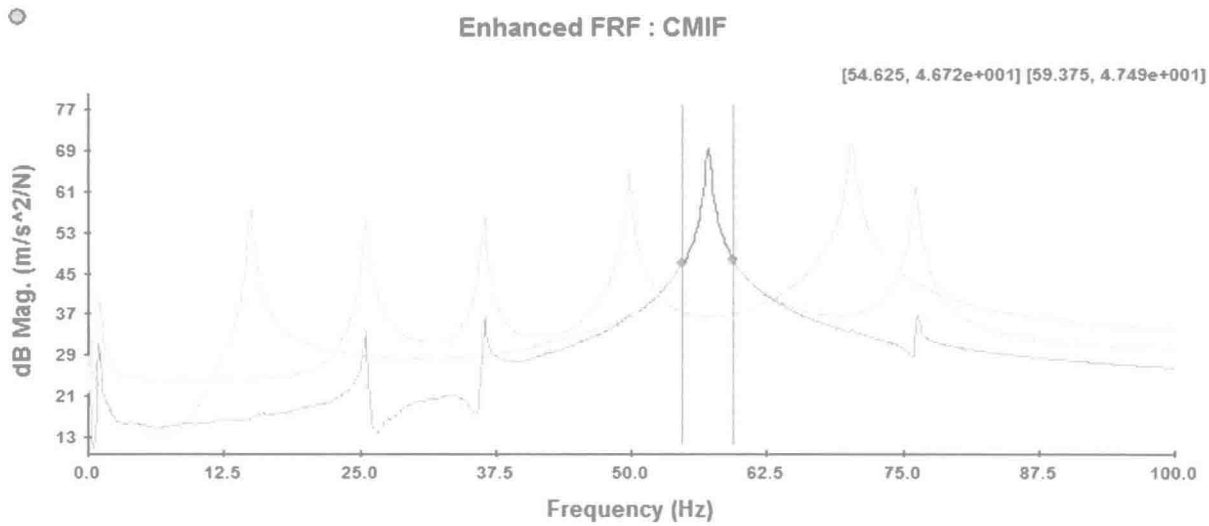

Fig. 1.3 One auto-determined fitting band in the enhance FRF of the aircraft model

Figure 1.4 shows the average mode indicator functions and the eight modes auto-detected by the presented peak-finding procedure. Figure 1.5 shows the first derivative of the mode indicator function. Figure 1.6 shows the enhanced PSD of the one mode at 0.7 Hz, in which the curve fitting band between two vertical lines is automatically determined by setting a MAC threshold of 0.7. The identified modal frequencies and damping ratios are shown in Table 1.2.

Table 1.1 Auto-identified modal parameters of the aircraft model

Mode	Frequency (Hz)	Damping (%)
1	0.92	0.84
2	14.92	0.30
3	25.56	0.30
4	36.41	0.15
5	49.75	0.13
6	57.08	0.17
7	70.27	0.21
8	76.16	0.14

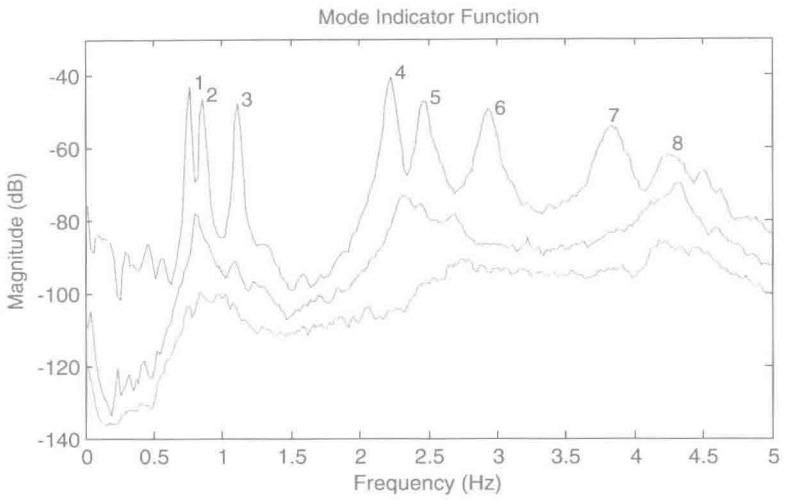

Fig. 1.4 Peaks found in the mode indicator function of the CFT building

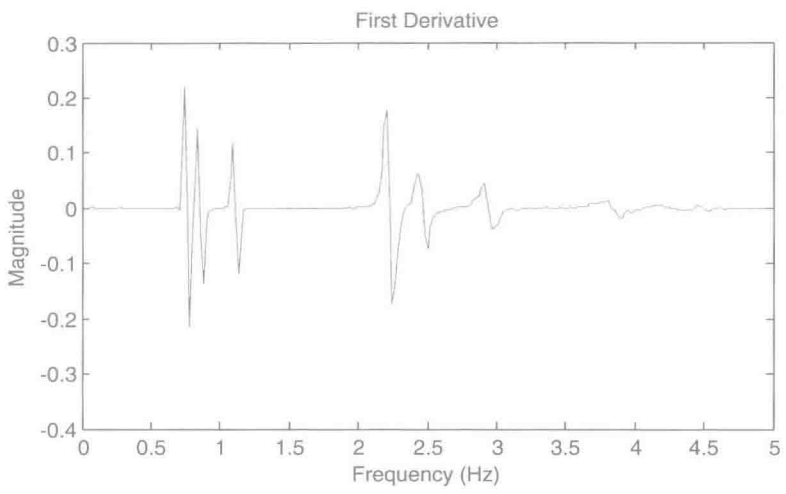

Fig. 1.5 First derivative of the mode indicator function of the CFT building

1.7 Conclusion

1. Two Narrow-Band identification methods, CMIF for experimental modal analysis, FSDD for operational modal analysis, are briefly reviewed.
2. The four-order Lagrange interpolation polynomial is applied to obtain the first derivative of the mode indicator function, from which the modal peaks can be automatically detected.

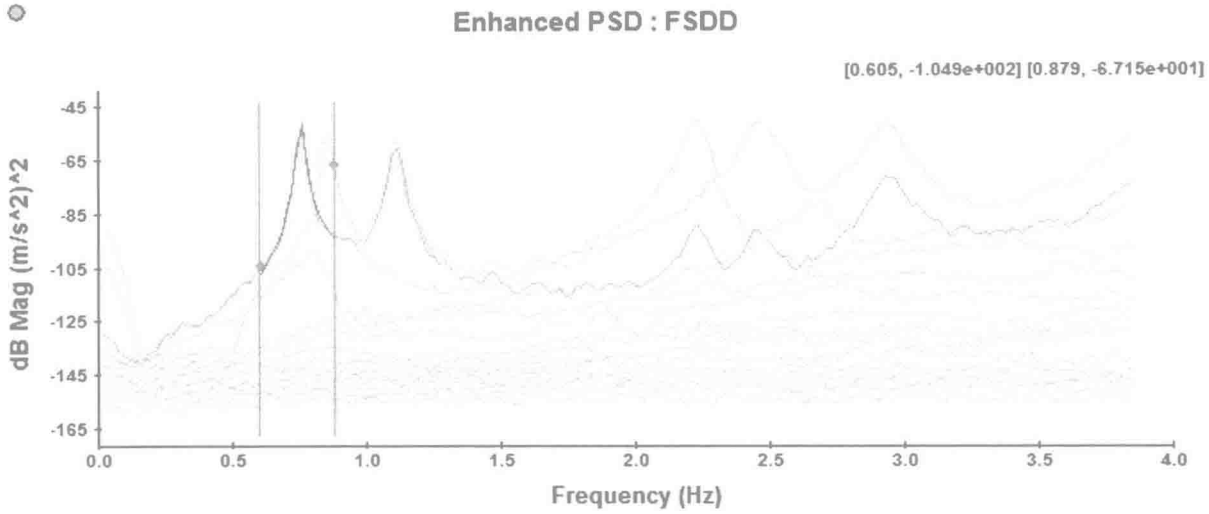

Fig. 1.6 One auto-determined fitting band in the enhance PSD of the CFT building

Table 1.2 Auto-identified modal parameters of the CFT building

Mode	Frequency (Hz)	Damping (%)
1	0.76	0.81
2	0.85	0.93
3	1.11	0.84
4	2.23	0.88
5	2.46	1.29
6	2.94	1.71
7	3.84	2.18
8	4.28	2.44

3. By calculating the MAC between the singular vector at the peak and the singular vector at the neighboring spectral lines, a fitting band in the enhanced FRF or PSD can be automatically to estimate the accurate modal frequency and damping ratio.
4. The auto-identification procedure was successfully applied to the experimental modal analysis of an aircraft model and to the operational modal analysis of a 15-story building.

Acknowledgement The support from NUAA Fundamental Research Funds NO. NN2012110 is gratefully acknowledged.

References

1. Shih CY, Tsuei YG et al (1989) Complex mode indication function and its applications to spatial domain parameter estimation. In: Proceeding of the 7th IMAC, Las Vegas, 1989
2. Wang T, Zhang LM (2006) Frequency and spatial domain decomposition for operational modal analysis and its application. Chin J Aeronaut 27(1):62–66
3. Zhang LM, Kanda H, Brown D, Allemang R (1985) A polyreference frequency domain method for modal parameter identification. ASME Paper, Number 85-DET-106
4. Van Der Auweraer H, Leuridan J (1987) Multiple input orthogonal polynomial parameter estimation. Mech Syst Signal Process 1(3):259–272
5. Guillaume P, Verboven P et al (2003) A poly-reference implementation of the least-squares complex frequency-domain estimator, IMAC 21. In: Proceeding of IMAC 21st, Kissimmee, February 2003
6. Zhang LM, Wang T, Tamura Y (2010) A frequency–spatial domain decomposition (FSDD) method for operational modal analysis. Mech Syst Signal Process 24(5):1227–1239
7. Andersen P, Brinker R et al (2007) Automated modal parameter estimation for operational modal analysis of large systems. In: The 2nd international operational modal analysis conference (IOMAC), Copenhagen, 2007

Chapter 2
Cable Parameters for Homogenous Cable-Beam Models for Space Structures

Kaitlin Spak, Gregory Agnes, and Daniel Inman

Abstract In this paper, a method to determine the effective homogenous beam parameters for a stranded cable is presented. There is not yet a predictive model for quantifying the structural impact of cable harnesses on space flight structures, and towards this goal, the authors aim to predict cable damping and resonance behavior. Cables can be modeled as shear beams, but the shear beam model assumes a homogenous, isotropic material, which a stranded cable is not. Thus, the cable-beam model requires calculation of effectively homogenous properties, including density, area, bending stiffness, and modulus of rigidity to predict the natural frequencies of the cable. Through a combination of measurement and correction factors, upper and lower bounds for effective cable properties are calculated and shown to be effective in a cable-beam model for natural frequency prediction.

Keywords Cable parameters • Cable modeling • Cable bending stiffness • Cable beam model • Cable vibration

Nomenclature

A	Cross-sectional area
c	Viscous damping coefficient
D	Cable outer diameter
d	Individual wire diameter
E	Elastic modulus
EI	Cable bending stiffness
F_s	Transfer function matrix for use in distributed transfer function method
G	Shear modulus
$G(s)$	Hysteretic damping function
I	Moment area of inertia
k	Spring stiffness, varies by cable size
L	Beam length
M, N	Left and right boundary condition matrices for distributed transfer function method
r	Layer diameter
Sys_m	System matrix
s	Laplace transformed time coordinate
T	Axial tension in cable
T_m	Transformation matrix
t	Time coordinate

K. Spak (✉)
Virginia Tech, Blacksburg, VA, USA
e-mail: kspak@vt.edu

G. Agnes
Jet Propulsion Laboratory, California Institute of Technology, Pasadena, CA, USA

D. Inman
Department of Aerospace Engineering, University of Michigan, Ann Arbor, MI, USA

F.N. Catbas (ed.), *Dynamics of Civil Structures, Volume 4: Proceedings of the 32nd IMAC, A Conference and Exposition on Structural Dynamics, 2014*, Conference Proceedings of the Society for Experimental Mechanics Series,
DOI 10.1007/978-3-319-04546-7_2,

V Volume fraction
w Beam displacement as a function of time and distance
x Spatial coordinate; distance along the beam in the axial direction
β Lay angle
η State space vector of displacement solution and derivatives for distributed transfer function method
κ Shear coefficient
ν Poisson's ratio
ρ Density
ϕ Angle between cable neutral axis and individual wire, as viewed from cable end
ψ Total beam rotation

2.1 Introduction

The control of space structures depends on accurate knowledge of their dynamic response to inputs. Thus, space structure models need to be high-fidelity and as realistic as possible to ensure accurate positioning. When lightweight structures are dressed with relatively heavy power and signal cables, the structures' dynamic response changes [1, 2]. In an effort to quantify and predict the dynamic response of cabled space structures, the study of cable dynamics is becoming increasingly important as requirements for dynamic mechanical stability of spacecraft become more stringent [3].

Cables used on spacecraft span a wide range of sizes, construction, and insulation. Currently, determination of cable parameters such as bending stiffness are performed experimentally through dynamic testing, and studies conducted to date used experimental data to back out the desired cable properties [4]. Ideally, cable parameters could be input into models based on basic measurements and properties of the cable rather than relying on experimental testing, which is more expensive and time consuming, and must be performed for each individual cable configuration. Therefore, this effort was conducted to determine how cable parameters could be simply calculated from wire measurements, material properties, and cable configuration.

In this paper, methods to determine cabled beam parameters a priori are presented. The cable parameters are used in a shear beam model to predict the natural frequencies of four types of cable. Comparison to experimental data to establish the validity of these methods concludes the paper.

2.2 Background

Cables can be modeled as shear beams [3]. Using a beam model is relatively straightforward and provides useful dynamic response data that can incorporate tension, internal damping and connection points. Beam models are not capable of determining internal friction forces directly, but instead rely on effective beam properties such as bending stiffness and damping to capture the frictional effects. Thus, determining these parameters to accurately portray the dynamic response is important.

The cables used for space structures are generally made of an aluminum or copper core surrounded by EMI shielding and some type of electrical insulation. A core wire surrounded by layer wires is known as a strand. Cables have a core wire or strand surrounded by helically twisted wires or strands in successive layers. An "m × n" designation is used to describe cable

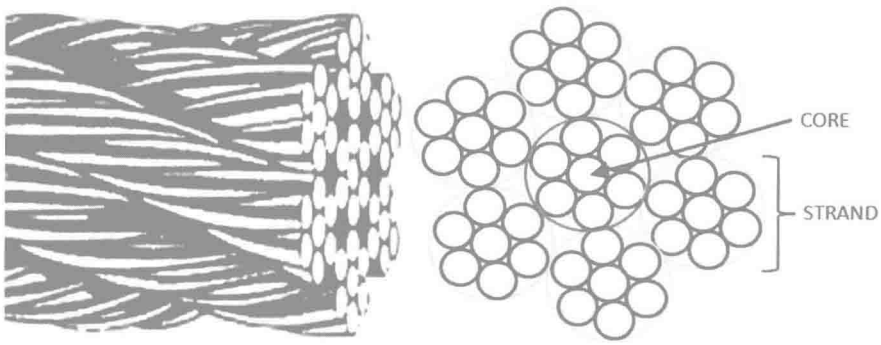

Fig. 2.1 A 7 × 7 multi-strand cable consisting of a 1 × 7 core strand surrounded by a single layer of 1 × 7 strands

configuration, in which m is the number of strands and n is the number of wires in each strand. Figure 2.1 shows the layout of a 7×7 stranded cable comprising a 1×7 core and six 1×7 layer strands. Cables made up of wires in multiple small strands are more flexible than cables made up of a single strand with the same total number of wires. Cables may be helically twisted, in which each layer is wrapped in the same direction, or contra-helically twisted, in which the wrapping direction alternates with each successive layer. The lay angle is the angle that the layer wires makes with the core; cable lay angles generally range from 2.5° to 35°, with most mathematical analysis of cable behavior departing from reality beyond 20° [5].

2.3 Cable Anatomy

The cable configurations investigated were 1×7, 1×19, 1×48, and 7×7, as shown in Fig. 2.2. Five samples of each cable type were used, which were provided at cost by Southern California Braiding, Inc, a manufacturer of space-flight compatible cables. The cables were manufactured and wrapped on a planetary machine which ensured repeatability and uniformity between each sample. A contra-helical lay was used so that the cables would lay as straight as possible and natural curvature would not be a factor in the overall cable bending behavior. Cables were tied every 4–6 in. and wrapped with an outer layer of Kapton.

All of the cables used in this study were made with MIL27500-26TG2T14 wire. This wire, commonly used for space applications, consists of two 26AWG twisted wire pairs individually insulated, an EMI shield made of tinned copper, and outer Tefzel (ETFE) insulation layer. Figure 2.3 shows the components that make up the individual wire that is bundled together to make the cable. Figure 2.4 shows an idealized layout of the wire used for calculations. The wire has a left hand (s) lay and is shrink-wrapped with the Tefzel insulation, so there is an evident twist to the wire. The maximum and minimum wire diameters resulting from the twisting effect are averaged to give the effective wire diameter of 2.5 mm used throughout the study. Wire size measurements were taken from published values when possible [6] and verified with actual measurement.

It is clear that the properties of the wire are different depending on whether the copper cores of the 26AWG wires are aligned with the horizontal (bending) axis or with the vertical axis.

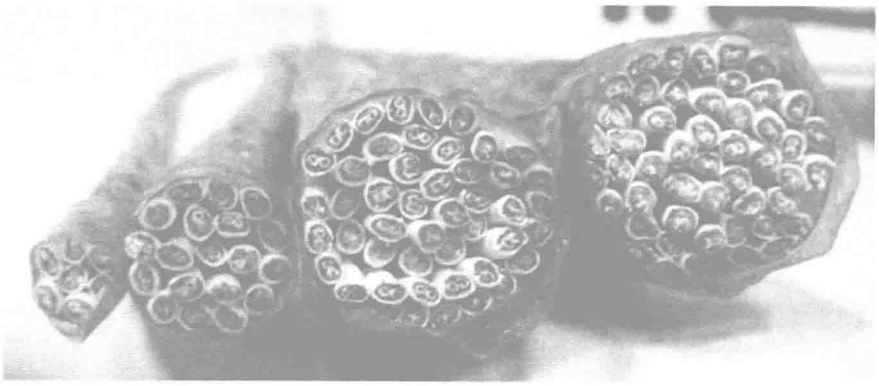

Fig. 2.2 Cable configurations investigated for this study; from *left* to *right*, 1×7, 1×19, 1×48, and 7×7

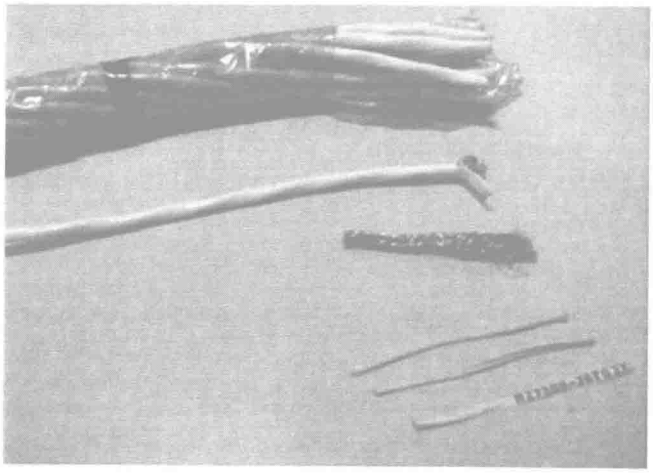

Fig. 2.3 Deconstructed cable wire, from *top* to *bottom*: Kapton wrapped cable, individual wire, and wire components: EMI shield, two 26AWG twisted wire pairs, and wire filler label

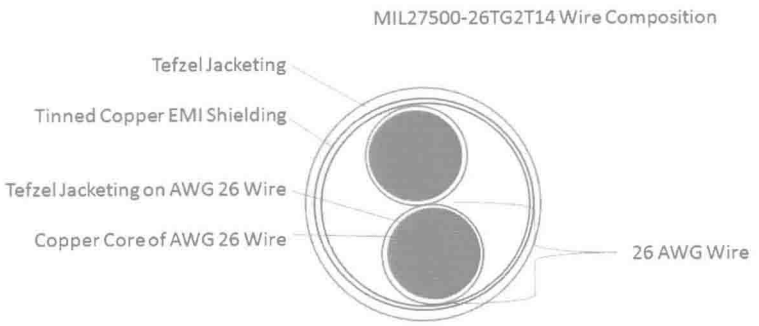

Fig. 2.4 Anatomy of MIL27500-26TG2T14 wire

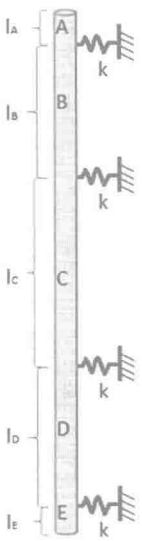

Fig. 2.5 DTFM cable model configuration

2.4 Beam Model

Although there are many ways to model helical cables, for the purposes of determining dynamic response and interaction between cables and structures, a beam model has many advantages. Instead of modeling the forces in between the wires, which is difficult at best, the beam model assumes that the cable can be modeled as a homogenous cylindrical beam, with damping incorporated through damping terms of various forms and variable bending stiffness. The difficulty lies in determining the homogenous beam parameters to use, since a stranded cable is certainly neither isotropic nor homogenous. Past studies have "smeared" the cable properties across each layer to some success [7].

Since the ultimate goal of this work is to determine the effect of cable harnesses on the damping and dynamics of space structures, a model that can eventually incorporate the cable connection points is desirable. Thus, the distributed transfer function method (DTFM) was used to solve the beam model derived from the equation of motion. The distributed transfer function method provides exact solutions for the dynamic response of both branched and un-branched systems without requiring calculation of the system eigensolutions [8]. For the cables investigated here, an un-branched system was used with five segments and four mounting points, following the method of Yang [9]. Figure 2.5 shows the model configuration, designed to mimic the experimental test setup in terms of cable segments and boundary conditions.

The equation of motion is put into state space form and is combined with boundary condition matrices to form the characteristic equation. For an un-branched system such as a straight cable, the characteristic equation consists of the exponential of the state space matrix and transition matrices that relate the sections and include the spring connections to ground as shown in Fig. 2.5.

To use the DTF method for a cable, the basic beam equation of motion is modified to include shear terms, a tension term, and damping terms (both viscous and hysteretic). The full equation of motion is:

$$\rho A\frac{\partial^2 w}{\partial t^2}-\frac{\rho E I}{\kappa G}\frac{\partial^4 w}{\partial t^2\partial x^2}+EI\frac{\partial^4 w}{\partial x^4}-\frac{cEI}{\kappa AG}\frac{\partial^3 w}{\partial t\partial x^2}-\int_0^t g(t-\tau)\frac{\partial^4 w}{\partial x^4}dt+c\frac{\partial w}{\partial t}+T\frac{\partial^2 w}{\partial x^2}=0$$